frontiers | Frontiers in Earth Science

TYPE Original Research
PUBLISHED 12 September 2022
DOI 10.3389/feart.2022.998061

OPEN ACCESS

EDITED BY
Zhiwei Xu,
Nanjing University, China

REVIEWED BY
Li Wu,
Anhui Normal University, China
Nannan Li,
Xiamen University, China
Ruijie Lu,
Beijing Normal University, China

*CORRESPONDENCE
Yixin Wang,
yixinw89@163.com

SPECIALTY SECTION
This article was submitted to Quaternary Science, Geomorphology and Paleoenvironment,
a section of the journal
Frontiers in Earth Science

RECEIVED 19 July 2022
ACCEPTED 10 August 2022
PUBLISHED 12 September 2022

CITATION
Wang Y, Ning K, He Q, Jie D and Guan Q (2022), Holocene paleotemperature reconstruction based on phytolith records of lacustrine sediments in the Badain Jaran Desert, northwestern China.
Front. Earth Sci. 10:998061.
doi: 10.3389/feart.2022.998061

Holocene paleotemperature reconstruction based on phytolith records of lacustrine sediments in the Badain Jaran Desert, northwestern China

Yixin Wang[1]*, Kai Ning[2], Qinghua He[1], Dongmei Jie[3] and Qingyu Guan[1]

[1]College of Earth and Environmental Sciences, Lanzhou University, Chengguan, Lanzhou, Gansu, China, [2]Institute of Hydrogeology and Environmental Geology, Chinese Academy of Geological Sciences, Shijiazhuang, Hebei, China, [3]School of Geographical Sciences, Northeast Normal University, Changchun, Jilin, China

Quantitative reconstruction of regional paleotemperature is the key to understanding temperature change and its driving mechanisms. In this study, 133 phytolith samples were collected as proxy indicators from lacustrine sediments of the Zhunzhahanjilin (ZZH) profile in the hinterland of the Badain Jaran Desert, China. The phytolith samples were then analyzed to quantitatively reconstruct the Holocene paleotemperature at the millennial scale. Based on accelerator mass spectrometry (AMS), ^{14}C dates and an ordered clustering method were used to divide the phytoliths into five assemblage zones with environmental significance. The quantitative reconstruction results indicated that the paleotemperature in the Badain Jaran Desert was relatively high during the early Holocene (11,040–8,200 cal a BP), and the average paleotemperature was approximately 9.5°C. This may have led to increased melt water near the surrounding area and recharged the lakes in the Badain Jaran Desert, resulting in the expansion of the lakes during the early Holocene. The average paleotemperature during the middle Holocene (8,200–3,100 cal a BP) was approximately 7.9°C. This period was warm and the environment was humid, with extensive precipitation from summer monsoons and low evaporation leading to higher water levels in the lakes. The paleotemperature decreased during the late Holocene (3,100 cal a BP to the present), and lakes retreated or dried up because of the decreased summer monsoon rains. The Holocene paleotemperature in the Badain Jaran Desert may have been related to July insolation in the Northern Hemisphere and had a range of impacts on the hydrological cycle in this arid region.

KEYWORDS

Badain Jaran Desert, dry land, phytoliths, holocene, paleotemperature

Introduction

With ongoing global warming (Wanner et al., 2008), global environmental problems have become exacerbated, and significantly greater attention is being placed on climate change research (IPCC, 2021). The Holocene was a critical period for human society entering the stage of civilization following the last glacial period. Therefore, the causes and process of Holocene climate change throughout this epoch have become one of the most important research areas for scholars.

Over the past 20 years, scholars have undertaken a preliminary paleoenvironmental reconstruction of the Badain Jaran Desert and its adjacent areas using multiple proxy-based reconstructions, such as the landscape (Yang, 2000), lake sediments (Yang et al., 2003), and calcareous root tubes and cores (Li et al., 2015a; Ning et al., 2021). Those studies have explored the mechanisms of environmental evolution (An et al., 2008; Zhao et al., 2008; Hartman and Wünnemann, 2009; Ning et al., 2019). However, detailed reconstructions of the desert environment have been quite limited, partly due to the poor preservation of biotic proxies and the complexity of the regional environment (Dong et al., 2010; Zhang H. et al., 2011; Li et al., 2017; Gao et al., 2020). There are still some uncertainties in the study of some characteristics of climate stages in environmental reconstruction, which are worthy of further systematic and thorough investigation. The Badain Jaran Desert is located in a climate-sensitive zone on the edge of the East Asian monsoon area. Due to low precipitation and high evaporation, there are 110 lakes recharged by groundwater in the southeastern part of the desert and no surface runoff in this region (Ma et al., 2014; Wang et al., 2016; Dong et al., 2022). This is an important region for studying environmental evolution and paleoclimate change (Wang et al., 2016; Li et al., 2018). Quantitative reconstruction of regional paleoclimate is the key to understanding climate change and its driving mechanism (Mohtadi et al., 2016).

Because quantitative temperature reconstructions in this area are very scarce, it is essential to find temperature records for Holocene climate change research in the desert hinterland of the Asian monsoon margin area (Gao et al., 2020). By comparing, checking, and synthesizing a variety of alternative data, some temperature series that can be used to reflect regional and global scales have been reconstructed (Yang et al., 2002; Mann and Jones, 2003; Ge et al., 2005; Moberg et al., 2006). According to substitute evidence from pollen, stalagmites, and lake deposition over the past 20 years, the temperature change sequences from 31 regions in China were reconstructed, which is of great significance for revealing climate change patterns and identifying the influence of human activities on modern climate warming (Ge et al., 2005). Fang and Hou (2011) used quantitative methods to reconstruct the centennial integrated temperature series resolution of the Holocene in China and divided the Holocene period into three stages.

Phytoliths are composed of an insoluble form of silica that precipitated within and between plant cells. They were formed by the uptake of soluble silicic acids from the soil through the roots, which were then transported to other parts of the plant (Wang and Lu, 1993; Blinnikov et al., 2002). Because the formation of phytoliths is deeply affected by environmental factors, they can be used as a good proxy for local vegetation, climate, and environmental conditions. Phytoliths can be well preserved in lacustrine deposits, peat deposits, paleosol strata or even sand dunes (Horrocks et al., 2000; Lu et al., 2007; Zhang et al., 2008; Gao et al., 2020). Moreover, they are poorly transported, relatively easily preserved, and can better reflect primary deposition, while maintaining a clear significance in terms of classification (Lu and Liu, 2003; Gao et al., 2018a). Phytoliths are widely used in the study of paleoenvironmental evolution. In China, researchers have undertaken various types of phytolith analyses, using phytolith assemblages, phytolith indices, and phytolith climate factor conversion functions to reconstruct the paleoclimate semi-quantitatively and quantitatively (Qiao et al., 2010; Gao et al., 2018b; Wang et al., 2019; Gao et al., 2020). Accordingly, phytoliths have been recognized as effective proxy indicators of climate change and have been widely used in paleoenvironment evolution research.

Overview of the study area

In the Badain Jaran Desert (39°20′–41°19′N, 99°54′–104°34′E), the geological structure of the desert forms part of the depression basin of the Alashan Platform, where the fracture is separated from the Alashan uplift on the west side of the Zongnai Mountains (Zhang J. et al., 2011). Analysis of distributed strata and structures revealed that the Badain Jaran area might have been integrated with the Alashan uplift in the Paleozoic era. When the fold/uplift was initiated from the Haixi movement, a fracture also occurred at the Alashan uplift (Wang, 1990). Its modern geomorphic features were formed under the backdrop of its overall aridity, including erosion from wind and flowing water as well as transportation and accumulation (Liu et al., 2010). The surface sediments of the desert are primarily composed of aeolian sediments and medium-fine sand (Ning et al., 2013). Mobile sand dunes are widely distributed, and the southeastern part of the desert maintains the highest and largest sand mountain group in the world (Niu et al., 2021).

The desert sustains seasonally frozen modern soils and has a temperate continental climate with extreme drought. The annual temperature difference is large (34.4°C), with an average summer temperature of 25.3°C and a winter temperature of −9.1°C (Ma et al., 2014). The Badain Jaran Desert is distant from the sea, receives little rain and suffers from perpetual drought. At the southern edge of the desert, the average annual precipitation is between 90.1 and 115.4 mm. At the northern edge of the desert, the annual average precipitation is between 35.2 and 42.9 mm, and the regional average precipitation is only 76.9 mm. The potential moisture loss from evapotranspiration is much higher than the water influx from

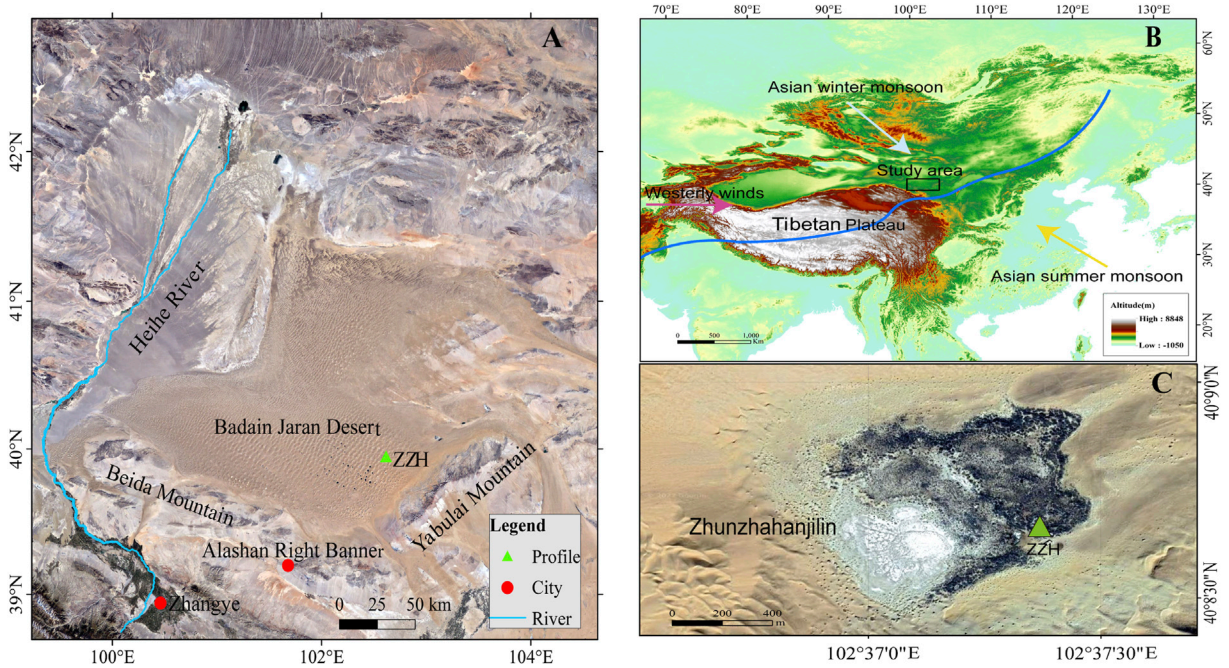

FIGURE 1
(A) Location of the ZZH profile in the southeastern part of the Badain Jaran Desert. **(B)** The black square on the map shows the location of the study area in northwestern China, and the blue line shows the limit of the Asian summer monsoon. The white arrow indicates the Asian winter monsoon, the yellow arrow indicates the Asian summer monsoon, and the purple arrow indicates the westerly winds. **(C)** The ZZH profile within the Zhunzhahanjilin arid lake basin.

precipitation (Ma et al., 2011). There is almost no surface runoff in the Badain Jaran Desert. For the more than 110 perennially stagnant lakes distributed in the southeast of the desert, as well as along the leeward slope of inter-dune depressions between the high sand mountains in the hinterland, the primary recharge source is groundwater (Wang et al., 2016).

Vegetation in the desert is sparse, primarily consisting of xerophytes, super xerophytic shrubs, and sub-shrubs, with predominantly annual herbaceous plants (Wang et al., 2015). The vegetation is distributed around the lake basins with marshy saline meadows near the water featuring several species, including *Glaux maritima*, *Trigolochin maritimum*, and *Aeluropus littoralis*. *Phragmites communis* and *Achnatherum splendens* are mainly constructive species confined to the periphery, beyond which are thicket and sand dunes dominated by white thorn (Wang et al., 2011).

In this study, we chose the Zhunzhahan Jilin (ZZH) profile for analysis, located in the depression of a seasonal stagnant lake in the hinterland of the Badain Jaran Desert (39°57′13″N, 102°37′13″E, 1,246 m a.s.l.) (Figure 1). ZZH is a dry lake basin with minimum run off and was not affected by the water level of the seasonal stagnant water depression. The depth of the profile is 3.9 m. It was excavated manually by our research team. The sampling along the profile was from top to bottom for less than 2 m, and from bottom to top for 2–3.85 m.

Materials and methods

Data source

The samples were collected to a depth of 385 cm in two parts: at 0–200 cm, with 2 cm sampling intervals (n = 99 samples; No. A1–A100, A20 missing), and at 200–385 cm, with 5 cm sampling intervals (n = 34 samples; No. B1, B2, B7–B38). The texture and color of the ZZH sedimentary faces were described as followed (Ning et al., 2019): 0–40 cm corresponds to a moderate consolidated sand layer with a grayish yellow color; 40–100 cm reflects the limnetic layer with a gray-black color; 100–125 cm represents rust spots in a yellow sand layer; 125–170 cm represents more silt in a gray-black silt limnetic layer; 175–348 cm, represents silt-sand with a yellow-green color. The 175–248 cm upper layer shows grayish-green rust spots in permanent yellowish-brown fine sand; the 248–348 cm under layer reflects grayish-green; at 348–385 cm, there are abundant plant residues mixed in a black peat layer; and, below 385 cm, there is a brown unconsolidated aeolian sand layer.

Seven samples for dating were collected from the profile, three were sent to the AMS dating laboratory of Peking University for determination, and the remaining four samples were pretreated and dated by BETA Analytic Inc. (Miami, FL, United States). The phytolith extraction for all of the 133 sediment samples was conducted at the School of Geographical Sciences, Northeast Normal University, Jilin, China. Ning et al. (2019) previously established a chronological sequence based on the AMS ^{14}C dating results for the ZZH profile in the Badain Jaran Desert.

Phytolith collection and classification

Experiment samples were treated using the wet ashing method (Lu et al., 2006; Gao et al., 2018c) according to the following steps: (1) Samples were dried and their weights recorded; (2) For oxidation, 25 g samples were placed in a centrifuge tube and dilute hydrochloric acid was added to remove the carbonate. The samples were washed with distilled water, and concentrated nitric acid was added to completely oxidize organic matter. (3) For heavy liquid flotation, a zinc bromide solution ('heavy liquid') with a specific gravity of 2.34 was added at a volume of more than 1.5 times that of the sample and centrifuged at 2000 rpm for 15 min. The upper suspension was removed to another centrifuge tube and distilled water was added for repeated centrifugal washing until the sample pH was neutral; (4) After flotation, the heavy liquids were cleaned, spores of known concentration (one spore tablet is about 27,640 grains) were added, dissolved with dilute HCl, and the samples were repeatedly washed until the pH was around 7; (5) The phytoliths were then identified and statistically categorized using permanent reference slides and an Olympus optical microscope. Through this analysis, 43,773 phytoliths were identified across the 133 samples from the ZZH profile. In general, the phytolith concentration from 0 to 162 cm was relatively high, (average, 473,000 grains·g^{-1}); whereas the concentration from 162 to 375 cm was comparatively low (average, 1,300 grains·g^{-1}). Calculation of the percent phytolith content was done according to the following formula:

$$p = n/s \times 100\% \tag{1}$$

where p is the percentage of each type of phytolith, n is the number of each phytolith type, and s is the total number of phytoliths counted.

$$C \equiv (s \times M)/(S \times m) \tag{2}$$

C is the concentration of phytoliths, s is the total number of phytoliths counted, M is the number of spores on each tablet, S is the total number of spores, and m is the sample weight.

Phytolith types were identified (Figures 2, 3) in the experiment. Most of the phytoliths were derived from Poaceae and Cyperaceae, with occasional ferns and Xylophyta also being present.

Quantitative temperature reconstruction

From the 133 sediment samples, a large number of phytoliths were observed, we selected ten of the most representative phytolith types, namely rondels, saddles, dumbbells, elongated, fans, long points, short points, rectangles, gobbets, and wavy (Lu et al., 2006). The remaining types were excluded due to their small numbers. We combined short saddles and long saddles into saddles, sinuate elongate and smooth elongate into elongate, and wavy-trapezoid and wavy narrow into wavy.

According to Lu et al. (2006), there were 243 sites with calibration sets for the modern surface sediment based on the wide ecological and climatic gradients in China. Therefore, we chose the 27 sites within the 243 surface sediments calibration set from Lu et al. (2006). The mean annual precipitation for these 27 sites was <200 mm which included the northwestern arid region in China. We then extracted the temperature data for these 27 sites in concert with the China meteorological forcing data (CMFD) during the time span of 1979–2018. This study applied the transfer function to the phytolith types from the ZZH profile in the Badain Jaran Desert; the R (*4.2.0*) package of "rioja" was selected for the modern training set of 27 sites from the data set of 243 surface sediments (Lu et al., 2006). First, the phytolith-inferred $MAT_{pre.\ 1}$ was the result of the weighted-averaging partial least squares regression (WA-PLS) model (Ter Break and Juggins, 1993), which extracted the most efficient component. The modern predicted temperature reconstruction ($MAT_{pre.\ 1}$) was then calculated in R [R^2_{boot} = 0.26, root-mean-square-error (RMSE) = 2.62]. Second, the $MAT_{pre.\ 1}$ was linearly fitted with CMFD ($MAT_{obs.\ 1}$) (known from 1979 to 2018) and a linear fitted equation was obtained. The inference data with the cross-validation are reflected by the $MAT_{obs.\ 1}$ and the $MAT_{pre.\ 1}$ had a statistical correlation (Figure 4). Third, the phytolith data in this study were substituted into the above model, and the Holocene paleotemperature reconstruction was obtained ($MAT_{pre.}$) [R^2_{boot} = 0.28, RMSE = 4.00]. Due to the value of R^2 ($MAT_{pre.}$) being relatively low, we used the linear fitted equation to obtain the results for the observed Holocene paleotemperature ($MAT_{obs.}$).

$$MAT_{obs.} = 1.02 \times MAT_{pre.} + 0.03 \tag{3}$$

where $MAT_{pre.}$ is the predicted Holocene paleotemperature, and $MAT_{obs.}$ is the observed Holocene paleotemperature.

Results

Based on the ordered clustering results of the percent phytolith content, the phytoliths were divided into five assemblage zones using Tilia (*v.1.7.16*) software which rendered the accompanying graph (Figure 5).

Zone I (385–325 cm) 11,040–9,800 cal a BP

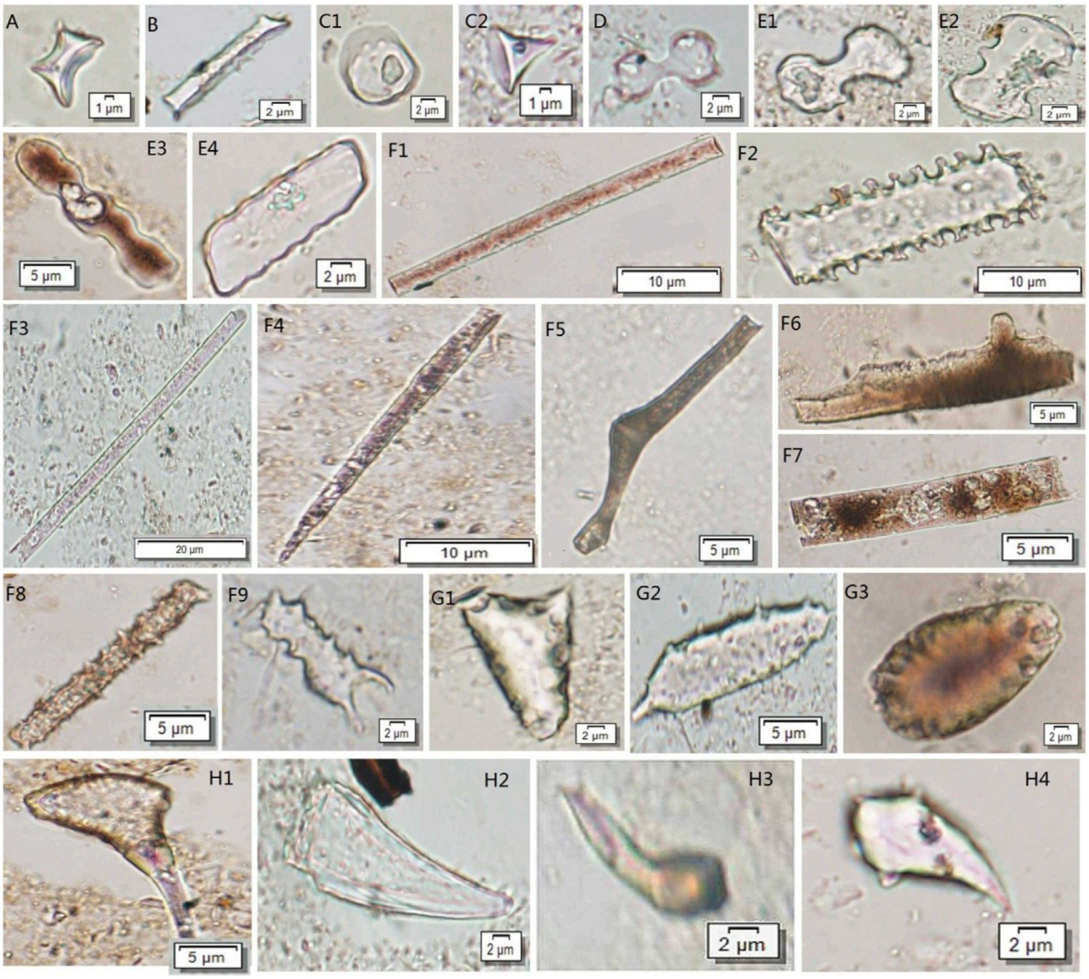

FIGURE 2
The phytolith morphology types from the ZZH profile in the Badain Jaran Desert. Saddles **(A,B)**; rondels **(C1,C2)**; dumbbells **(D)**; wavy **(E1–E4)**; elongated **(F1–F9)**; short points **(G1–G3)**; long points **(H1–H4)**.

The phytolith assemblages in zone I were dominated by gobbets (38.8–59.0%, avg. content = 48.0%) and elongated (16.9–28.0%, avg. content = 21.0%). The percent contents of rondels (7.8–18.7%, avg. content = 12.8%), rectangles (3.8–13.1%, avg. content = 8.0%) and short points (3.4–7.3%, avg. content = 5.2%) were relatively high. Meanwhile, those of fans (1.3–5.6%, avg. content = 3.5%) and the average content of the remaining phytoliths, wavy, saddles, dumbbells, and long points were relatively low. The reconstructed $MAT_{obs.}$ was from 9.5 to 10.8°C during this period, and the average paleotemperature was 10.1°C.

Zone II (325–270 cm) 9,800–8,200 cal a BP

The phytolith assemblages from zone II were dominated by gobbets (39–50.4%, avg. content = 44.7%) and elongated (19.0–27.2%, avg. content = 23.8%), these two phytolith types showed a less pronounced decrease than in zone I. The percent content of rondels (10.5–18.7%, avg. content = 13.4%), short points (3.5–11.9%, avg. content = 7.4%) and fans (2.5–7.6%, avg. content = 5.4%) was slightly increased. The average content of rectangles decreased to 4.5%. The percent contents of wavy, dumbbells, and long points were relatively low. The reconstructed $MAT_{obs.}$ ranged from 7.4 to 10.4°C during this period, and the average paleotemperature was 8.8°C.

Zone III (270–144 cm) 8,200–3,100 cal a BP

According to the variation in the phytoliths, the phytolith assemblages of zone III were divided into two sub-zones.

Sub-zone III–A (270–190 cm) 8,200–4,500 cal a BP and Sub-zone IV–A were dominated by gobbets (27.5–50.7%, avg. content = 41.8%) and elongated (16.0–30.5%, avg. content =

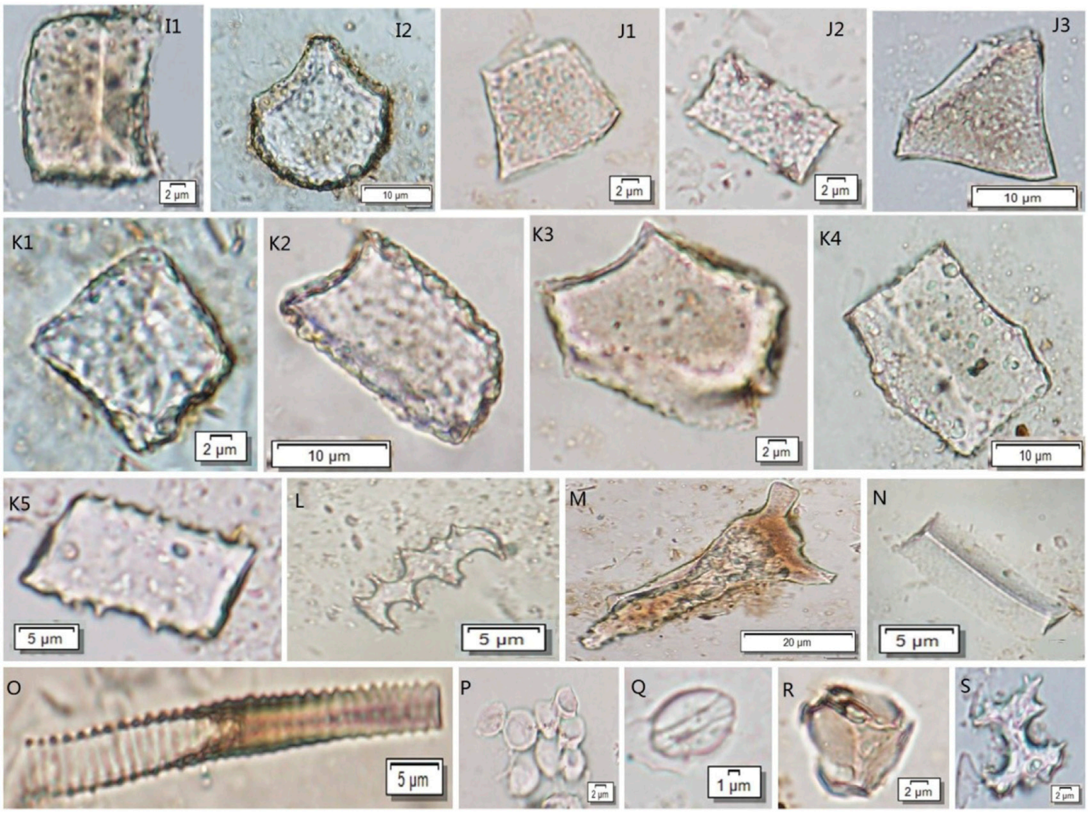

FIGURE 3
The phytolith morphology types from the ZZH profile in the Badain Jaran Desert. Fans **(I1,I2)**; rectangles **(J1–J3)**; gobbets **(K1–K5)**; **(L)** carinate; **(M)** brachiate; **(N)** prismatic; **(O)** silicified tracheids; **(P)** silicified plant tissue; **(Q)** silicified stomata; **(R)** epidermal phytolith; **(S)** special type.

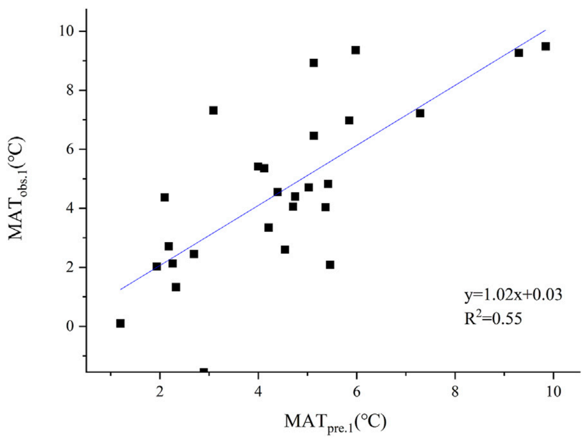

FIGURE 4
Relationships between the $MAT_{obs.\ 1}$ and $MAT_{pre.\ 1}$ The blue line represents the linear trend. This is significant at $p<0.01$.

22.2%). Rondels (10.2–24.1%, avg. content = 14.8%), short points (4.2–13.6%, avg. content = 8.8%), fans (2.3–10.7%, avg. content = 6.4%) and rectangles (2.3–7.4%, avg. content = 4.2) were in the middle level. The average contents of wavy and saddles were relatively low. The reconstructed $MAT_{obs.}$ ranged from 6.2 to 9.7°C during this period and the average paleotemperature was 8.0°C.

Sub-zone III–B (190–144 cm) 4,500–3,100 cal a BP and Sub-zone IV–B were dominated by gobbets (30.8–59.5%, avg. content = 42%) and elongated (14.8–31.3%, avg. content = 24.1%). The percent contents of fans (6.1–26.8%, avg. content = 12.4%) and short points (3.9–28.1%, avg. content = 9.2%) were relatively high. Rondels (0.7–18.8%, avg. content = 7.2%) showed a pronounced decrease. The percent contents of the remainder of the phytolith types were relatively low. The reconstructed $MAT_{obs.}$ ranged from 2.4 to 9.7°C during this period and the average paleotemperature was 7.7°C.

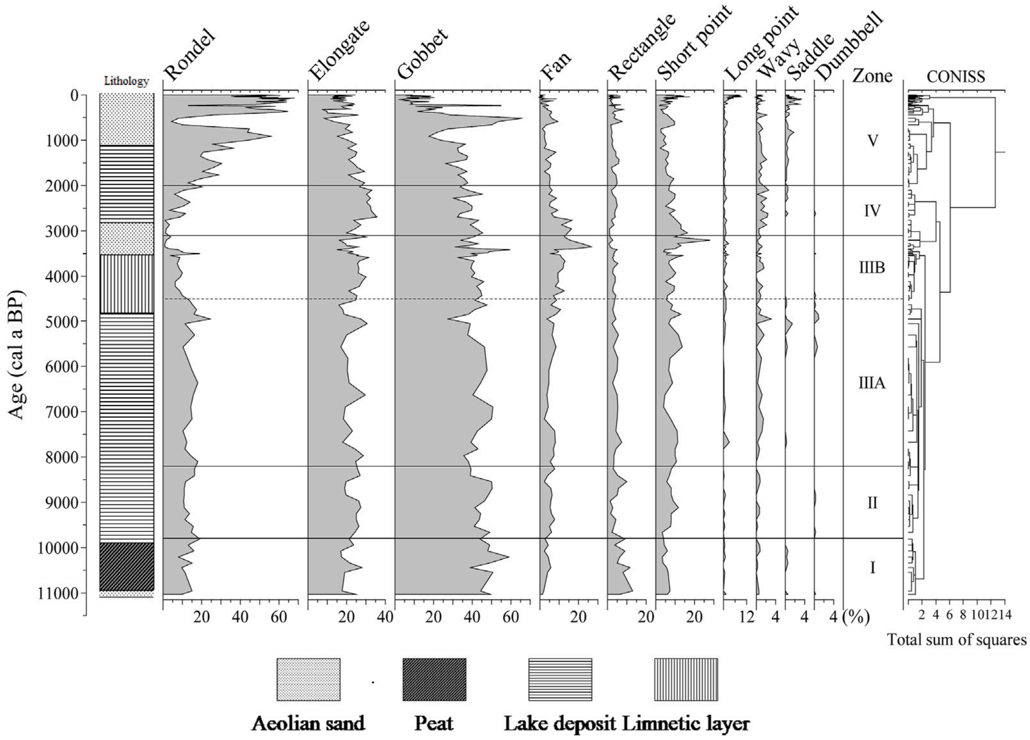

FIGURE 5
Phytolith assemblage observed from ZZH profile in the Badain Jaran Desert. Zone I, zone II, zone III, zone IV, and zone V indicate the 11–9.8 cal ka BP, 9.8–8.2 cal ka BP, 8.2–3.1 cal ka BP, 3.1–2 cal ka BP, and 2 cal ka BP to the present, respectively.

Zone IV (144–118 cm) 3,100–2000 cal a BP

The phytolith assemblages of zone IV were dominated by gobbets (30.2–45.2%, avg. content = 38.5%) and elongated (19.8–35.8%, avg. content = 29.4%). The percentage content of rondels (0.9–20%, avg. content = 7.4%), short points (5.2–16.2%, avg. content = 9.7%), and fans (4.7–16.6%, avg. content = 9.3) were relatively high. The percent contents of the remainder of the phytolith types were relatively low. The reconstructed $MAT_{obs.}$ ranged from 5.5 to 9.6°C during this period and the average paleotemperature was 7.8°C.

Zone V (118–0 cm) 2000 cal a BP to the present

The phytolith assemblages of zone V were dominated by rondels (4.2–68.0%, avg. content = 43.0%) and gobbets (3.0–65.9%, avg. content = 20.8%). The percent content of elongated (7.6–29.4%, avg. content = 18.5%) was relatively high and that of short points (2.2–17.7%, avg. content = 7.1%) and fans (0–9.3%, avg. content = 2.9%) were relatively low. The percent contents of the rest of the phytolith types were relatively low. The reconstructed $MAT_{obs.}$ ranged from 3.5 to 10°C during this period and the average paleotemperature was 6.6°C.

From the above results, we can see that the average paleotemperature during 11,040–9,800 cal a BP was 10.1°C, and the paleotemperature during 9,800–8,200 cal a BP was 8.8°C. We regarded these two periods as the early Holocene, with an average paleotemperature of approximately 9.5°C. While the paleotemperature during 8,200–3,100 cal a BP (sub-zone III-A, 8,200–4,500 cal a BP; sub-zone III-B, 4,500–3,100 cal a BP, with paleotemperature of 8.0 and 7.7°C, respectively) was 7.9°C, we regard this period as being the middle Holocene. The late Holocene was after 3,100 cal a BP and the average paleotemperature was 7.2°C.

Discussion

Comparison of paleotemperature changes during the Holocene in different regions

Many other Holocene climate records have been obtained from some arid regions in China. However, the timing and mechanisms of climate change during the Holocene is still being debated (Long et al., 2014). The phytolith-based paleotemperature reconstruction for the Badain Jaran Desert may provide more reliable information for the paleoclimate record. We compared the reconstructed paleotemperatures for different regions in China using various proxies. Based on the reconstructed temperature sequence, Fang

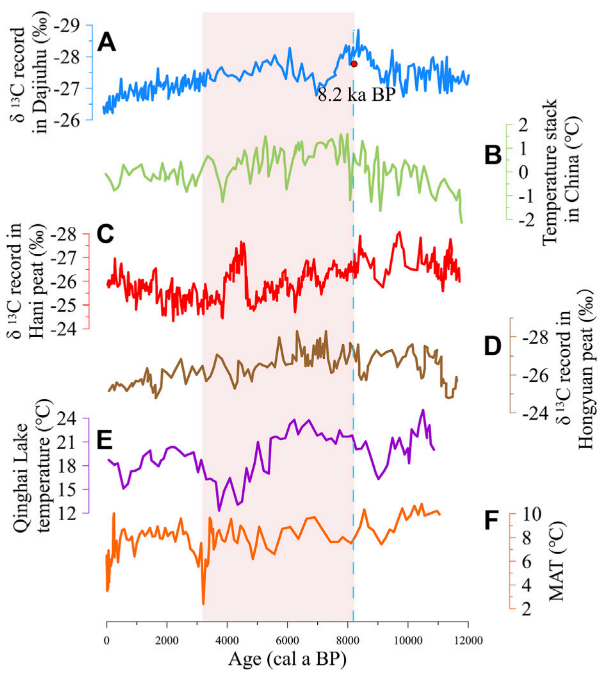

FIGURE 6
Comparison of Holocene temperature sequences in different regions. **(A)** $\delta^{13}C$ in the Dajiuhu peat of Shennongjia (Ma et al., 2008); **(B)** Temperature stack of China (Fang and Hou, 2011); **(C)** $\delta^{13}C$ record in the Hani peat, northeastern China (Hong et al., 2005); **(D)** $\delta^{13}C$ record in the Hongyuan peat, eastern Tibetan Plateau (Hong et al., 2003); **(E)** Qinghai Lake temperature (Hou et al., 2016); **(F)** the reconstructed temperature during the Holocene in the Badain Jaran Desert (this study). The pink area is the Holocene 'megathermal'. The red circle and the dotted blue line represent the cold event at 8.2 ka BP.

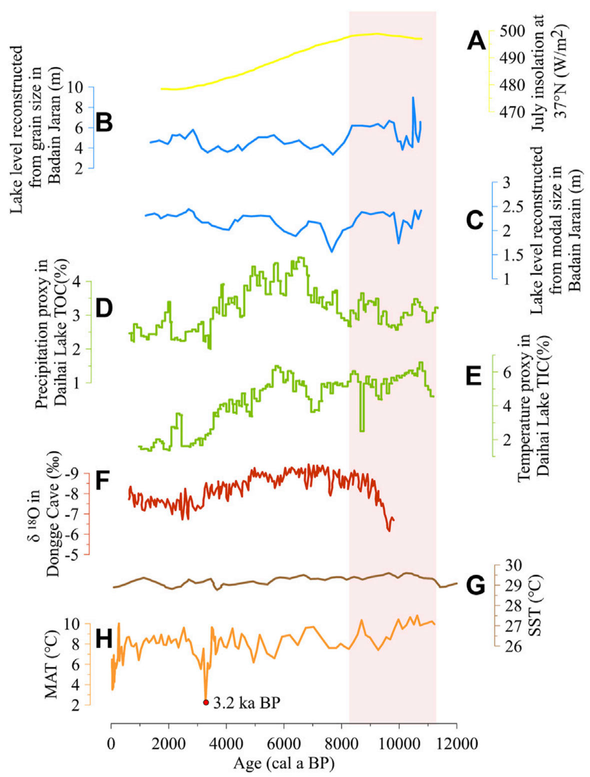

FIGURE 7
Quantitative reconstructions based on the phytolith of millennial-scale temperature changes in the Badain Jaran Desert during the Holocene and comparison with other Holocene records. **(A)** July insolation at 37°N (Laskar et al., 2004); **(B)** Lake level reconstructed from grain size in the Badain Jaran Desert (Dong et al., 2022); **(C)** Lake level reconstructed from modal size in the Badain Jaran Desert (Dong et al., 2022); **(D)** precipitation proxy in the Daihai Lake (Xiao et al., 2006); **(E)** temperature proxy in the Daihai Lake (Xiao et al., 2006); **(F)** $\delta^{18}O$ in the Dongge Cave, Guizhou Province, China (Dykoski et al., 2005); **(G)** sea surface temperature (SST) in the western tropical Pacific (Stott et al., 2004); **(H)** the reconstructed temperature in the Badain Jaran Desert (this study). The pink area represents the high paleotemperature in the early Holocene and the red circle represents the 3.2 ka BP event.

and Hou (2011) divided the Holocene paleotemperature into three stages in China, corresponding to the early, middle, and late Holocene. The paleotemperature during the early Holocene (11.5–8.9 ka BP) was fluctuating and increased and was approximately 1°C higher than in modern times. The paleotemperature in the middle Holocene (8.9–4.0 ka BP) reached its warmest peak during this period (8.0–6.4 ka BP). In the late Holocene (4.0 ka BP to the present), the paleotemperature decreased and the climate became cold (Figure 6B). Based on the geochemistry record of $\delta^{13}C$ in Dajiuhu peat by Ma et al. (2008), the early Holocene was cold, but the paleotemperature gradually increased. The middle Holocene was warm overall, but the representative cold event at 8.2 ka BP was strongly reflected, and the paleotemperature changed from warm to cold during the late Holocene (Figure 6A). We also compared the $\delta^{13}C$ record from the Hani peat (Hong et al., 2005) in northeastern China (Figure 6C) and the Hongyuan peat on the Tibetan Plateau (Hong et al., 2003) (Figure 6D), which was found to be similar to the Dajiuhu peat record. The pollen record in Daihai Lake (Xiao et al., 2004) also revealed the history of paleotemperature change during the Holocene in this region. From 10,250 to 7,900 ka BP, an increasing proportion of tree pollen implied that the environment had become warmer. Between 7,900 and 4,450 ka BP, the percentage of tree pollen reached its maximum value and the paleotemperature fluctuated but was relatively warm overall. During the period of 4,450 to 2,900 ka BP, tree pollen appeared and there was a sharp cooling with the paleotemperature dropping lower than in the previous period. In addition, the paleotemperature variation trend for the Qinghai Lake (Hou et al., 2016) (Figure 6E) showed results similar to our reconstructed MAT (Figure 6F). Hafsten (1970) also put forward the term 'megathermal' to explain the warmest period in the middle Holocene (8.2–3 ka BP). The data of the sediment core indicated that the Holocene megathermal was an arid period in Inner

Mongolia (Chen et al., 2003). The above research suggests that the middle Holocene was the warmest period during the epoch.

From the TIC and TOC sediment records from Daihai lake, Xiao et al. (2006) found that the climate of the early Holocene (11,500–8,100 ka BP) was warm and dry, whereas the middle Holocene (8,100–3,300 ka BP) was warm and wet due to the high TIC and TOC values, and during the late Holocene the climate became cold and dry (Figures 7D,E). Chen et al. (2008) hold the opinion that the Holocene climate in arid central Asia was driven by the surface sea temperature in the North Atlantic, the waning ice-sheets in the northern Hemisphere, the high air temperature at mid-latitudes, and the high degree of summer insolation. Our research found that the Holocene paleotemperature in the Badain Jaran Desert was similar to the sea surface temperature (SST) in the western tropical pacific (WTP) which has been reconstructed using Mg/Ca data and oxygen isotope levels from foraminifers extracted from sediment cores (Stott et al., 2004) (Figure 7G). From the $\delta^{18}O$ record in the Dongge Cave, China (Figure 7F), Dykoski et al. (2005) found that the Asian monsoon intensity generally correlated with the insolation changes, and our results were similar to the solar forcing mechanism in the Northern Hemisphere (Laskar et al., 2004) (Figure 7A). Peng et al. (2016) considered that the peak in Northern Hemisphere summer insolation was from 12 to 10 ka, correlating with the dune mobility in the Tengger Desert and other sand fields. This phenomenon might correlate with the strengthening of the Asian summer monsoon. This evidence could support our results that there were high paleotemperatures during the early Holocene.

The influence of paleotemperature on the hydrological cycle during the Holocene

The high paleotemperature during the early Holocene may have caused the high lake level and relative humid environment in the Badain Jaran Desert. In the early Holocene, the global temperature began to rise as solar radiation increased in the Northern Hemisphere, and the Badain Jaran Desert responded accordingly. Some researchers suggested that groundwater recharge was an important factor in lake-level changes in the Badain Jaran Desert. This is because groundwater recharge contributes 90% of the water balance, while precipitation contributes only 10% to the lake replenishment (Ma et al., 2014; Dong et al., 2016; Sun et al., 2018; Dong et al., 2022). The pan-lake period of Badain Jaran began in the early Holocene at 10 ka BP (Wang et al., 2016). This phenomenon can be attributed to increasing meltwater from the Qilian Mountains and the Tibetan Plateau, which is controlled by solar radiation in the Northern Hemisphere, and the high paleotemperature during the early Holocene. Thus, a considerable amount of meltwater flowed into the ground and became groundwater (Wu et al., 2004; Dong et al., 2022), while the glacier meltwater and precipitation in the northeastern Tibetan Plateau provided a large volume of groundwater to the Badain Jaran Desert (Ning et al., 2019). According to Dong et al. (2022), the lake level frequently fluctuated between 3.82 and 9.21 m during the early Holocene (10.6–8.6 ka BP) and slightly fluctuated between 3.41 and 5.26 m during the middle Holocene (8.6–4.7 ka BP) (Figure 7B,C). The literature examined in this discussion could further explain the hypothesis that the high temperature in the early Holocene led to lake expansion in the Badain Jaran Desert.

Li et al. (2015b) indicated that calcareous root tubes predominantly formed in environments with high relative humidity and could not form in an arid environment. Therefore, they found that the frequency of calcareous tubes was mainly concentrated in the middle Holocene in the Badain Jaran Desert, and their presence suggested that the middle Holocene was relatively humid. The strengthened summer monsoon also resulted in increased moisture in the middle Holocene (Yang et al., 2011). Ning et al. (2019) found that the concentration of n-alkanes was higher in the humid environment from 7.8 to 5.8 ka in the Badain Jaran Desert, which indicated the presence of a relatively wet environment during the middle Holocene. Moreover, when we referred to the pollen of *Artemisia* and Chenopodiaceae in arid areas, their A/C ratio proved that they afforded a reliable proxy for relative humidity (Zhao et al., 2012). Thus Ning et al. (2021) posited that the highest A/C ratio, between 7.2 and 5.4 ka, explained the high humidity conditions in the Badain Jaran Desert during the middle Holocene. During 7.7–5.3 ka BP, precipitation reached 200 mm yr^{-1} in the Badain Jaran Desert (Wang et al., 2016). Combined with our MAT data and the above evidence, we have deduced that the middle Holocene period was warm and wet and that this was due to extensive precipitation from the summer monsoon and the low evaporation in the desert (Li et al., 2015b; Wang et al., 2016; Ning et al., 2019; Dong et al., 2022), which had a strong impact on the high lake levels during this period.

During the late Holocene, many lakes retreated or dried up in the Badain Jaran Desert (Wang et al., 2016). This may have been caused by weak summer monsoons (Yang et al., 2010) along with human activities. From our MAT results, at approximately 3,200 ka BP, there was a sharp decrease in temperature, which may be a result of the neoglacial period (Cheng et al., 2020) or the arrival of the late Neolithic age.

Conclusions

Abundant phytoliths were found in the Zhunzhahan Jilin (ZZH) lacustrine sediments of the Badain Jaran Desert. Phytolith records provide a rich resource of information on Holocene climate changes and are particularly useful proxies for reconstructing the MAT in the Holocene.

Our results suggested that the temperature in the study area was relatively warm during the early Holocene, and the middle Holocene was not only warm but also humid, whereas it became cold in the late Holocene. The Holocene paleotemperature had an impact on the hydrological cycle and evolution of the lake group. During the early Holocene, the melt water recharged the groundwater and resulted in the swelling of lake groups. During the middle Holocene, the extensive precipitation from the summer monsoons led to high lake levels. During the late Holocene, however, the weak summer monsoons caused the lakes to retreat or dry up. These findings are consistent with the characteristics of climate evolution at the millennium scale in northern China. The mechanism of paleotemperature change in the Badain Jaran Desert was controlled by periodic changes in July insolation at 37°N.

More reliable inferences for the Holocene paleotemperature change will be obtained from more detailed records in the Badain Jaran Desert or nearby regions. Better information collection is needed for paleotemperature research approaches to better understand the characteristics and evolution of the Holocene environment and to provide a scientific basis for human adaptation to environmental change in the future.

Data availability statement

The original contributions presented in the study are included in the article, and any further inquiries can be directed to the corresponding author.

Author contributions

YW wrote the manuscript, contributed to the conception, and processed data. KN and QH did the fieldwork. DJ processed data and QG revised the manuscript. YW, KN, QH, and QG reviewed and edited the manuscript. All authors contributed to manuscript revision and discussion and approved the submitted version.

Funding

This work was supported by the National Natural Science Foundation of China (No. 41871021), the Fundamental Research Funds for the Central Universities (No. lzujbky-2018-it82), and the Basic Research Foundation of the Institute of Hydrogeology and Environmental Geology, Chinese Academy of Geological Sciences (No. SK202012).

Acknowledgments

We thank Lvlv Zhang and Xianbao Su for their assistance with field work.

Conflict of interest

The authors declare that the research was conducted in the absence of any commercial or financial relationships that could be construed as a potential conflict of interest.

Publisher's note

All claims expressed in this article are solely those of the authors and do not necessarily represent those of their affiliated organizations, or those of the publisher, the editors and the reviewers. Any product that may be evaluated in this article, or claim that may be made by its manufacturer, is not guaranteed or endorsed by the publisher.

References

An, C., Chen, F., and Barton, L. (2008). Holocene environmental changes in Mongolia: A review. *Glob. Planet. Change* 63 (4), 283–289. doi:10.1016/j.gloplacha.2008.03.007

Blinnikov, M., Busacca, A., and Whitlock, C. (2002). Reconstruction of the late pleistocene grassland of the columbia basin, Washington, USA, based on phytolith records in loess. *Palaeogeogr. Palaeoclimatol. Palaeoecol.* 177 (1–2), 77–101. doi:10.1016/S0031-0182(01)00353-4

Chen, C.-T. A., Lan, H., Lou, J., and Chen, Y. (2003). The dry Holocene megathermal in inner Mongolia. *Palaeogeogr. Palaeoclimatol. Palaeoecol.* 193 (2), 181–200. doi:10.1016/S0031-0182(03)00225-6

Chen, F., Yu, Z., Yang, M., Ito, E., Wang, S., Madsen, D. B., et al. (2008). Holocene moisture evolution in arid central Asia and its out-of-phase relationship with asian monsoon history. *Quat. Sci. Rev.* 27 (3–4), 351–364. doi:10.1016/j.quascirev.2007.10.017

Cheng, B., Adams, J., Chen, J.-H., Zhou, A., Zhang, Q., and Mackay, A. W. (2020). Neoglacial trends in diatom dynamics from a small alpine lake in the Qinling mountains of central China. *Clim. Past.* 16 (2), 543–554. doi:10.5194/cp-16-543-2020

Dong, C., Wang, N., Chen, J., Li, Z., Chen, H.-B., Chen, L., et al. (2016). New observational and experimental evidence for the recharge mechanism of the lake group in the alxa desert, north-Central China. *J. Arid. Environ.* 124, 48–61. doi:10.1016/j.jaridenv.2015.07.008

Dong, S., Li, Z., Li, M., Lu, C., Wang, N., and Ning, K. (2022). Quantitative reconstruction of consecutive paleolake-level fluctuations by the groundwater recharged lake in the desert hinterland: A case study in the Badain Jaran desert, northwestern China. *Catena* 212, 106051. doi:10.1016/j.catena.2022.106051

Dong, Z., Man, D., Luo, W., Qian, G., Wang, J., Zhao, M., et al. (2010). Horizontal aeolian sediment flux in the Minqin area, a major source of Chinese dust storms. *Geomorphology* 116 (1–2), 58–66. doi:10.1016/j.geomorph.2009.10.008

Dykoski, C. A., Edward, R. L., Cheng, H., Yuan, D., Cai, Y., Zhang, M., et al. (2005). A high-resolution, absolute-dated Holocene and deglacial Asian monsoon record from Dongge Cave, China. *Earth Planet. Sci. Lett.* 233 (1–2), 71–86. doi:10.1016/j.epsl.2005.01.036

Fang, X., and Hou, G. (2011). Synthetically reconstructed Holocene temperature change in China. *Sci. Geogr. Sin.* 31 (4), 385–393. doi:10.13249/j.cnki.sgs.2011.04.013

Gao, G., Jie, D., Li, D., Li, N., Liu, L., Shi, J., et al. (2018c). Reliability of phytoliths for reconstructing vegetation dynamics in northern temperate forest regions: A case study in northeast China. *Quat. Sci. Rev.* 201, 1–12. doi:10.1016/j.quascirev.2018.10.020

Gao, G., Jie, D., Liu, L., Liu, H., Li, D., Li, N., et al. (2018b). Assessment and calibration of representational bias in soil phytolith assemblages in northeast China and its implications for paleovegetation reconstruction. *Quat. Res.* 90 (1), 38–49. doi:10.1017/qua.2018.5

Gao, G., Jie, D., Wang, Y., Liu, L., Liu, H., Li, D., et al. (2018a). Do soil phytoliths accurately represent plant communities in a temperate region? A case study of Northeast China. *Veg. Hist. Archaeobot.* 27 (6), 753–765. doi:10.1007/s00334-018-0670-2

Gao, Y., Li, Z., Zhu, R., and Wang, N. (2020). Quantitative reconstruction of Holocene millennial scale precipitation in the asian monsoon margin of northwest China, revealed by phytolith assemblages from calcareous root tubes in the Tengger Desert. *Clim. Dyn.* 55 (3–4), 755–770. doi:10.1007/s00382-020-05293-4

Ge, Q., Wang, S., and Zheng, J. (2005). Reconstruction of temperature series in China during the past 5000 years. *Prog. Nat. Sci.* 16 (6), 689–696. doi:10.3321/j.issn:1002-008X.2006.06.008

Hafsten, U. (1970). A sub-division of the late pleistocene period on asynchronous basis, intended for global and universal usage. *Palaeogeogr. Palaeoclimatol. Palaeoecol.* 7 (4), 279–296. doi:10.1016/0031-0182(70)90097-0

Hartmann, K., and Wünnemann, B. (2009). Hydrological changes and Holocene climate variations in NW China, inferred from lake sediments of juyanze palaeolake by factor Analyses. *Quat. Int.* 194, 28–44. doi:10.1016/j.quaint.2007.06.037

Hong, Y., Hong, B., Lin, Q., Shibata, Y., Hirota, M., Zhu, Y., et al. (2005). Inverse phase oscillations between the East asian and Indian ocean summer monsoons during the last 12000 Years and paleo-el nino. *Earth Planet. Sci. Lett.* 231 (3–4), 337–346. doi:10.1016/j.epsl.2004.12.025

Hong, Y., Hong, B., Lin, Q., Zhu, Y., Shibata, Y., Hirota, M., et al. (2003). Correlation between Indian ocean summer monsoon and North Atlantic climate during the Holocene. *Earth Planet. Sci. Lett.* 211 (3–4), 371–380. doi:10.1016/S0012-821X(03)00207-3

Horrocks, M., Deng, Y., Ogden, J., and Sutton, D. G. (2000). A reconstruction of the history of a Holocene sand dune on great barrier island, northern New Zealand, using pollen and phytolith analyses. *J. Biogeogr.* 27 (6), 1269–1277. doi:10.1046/j.1365-2699.2000.00508.x

Hou, J., Huang, Y., Zhao, J., Liu, Z., Colman, S., and An, Z. (2016). Large Holocene summer temperature oscillations and impact on the peopling of the northeastern Tibetan plateau. *Geophys. Res. Lett.* 43 (3), 1323–1330. doi:10.1002/2015GL067317

IPCC (2021). *Climate change 2021 the physical science basis: Working group I contribution to the sixth assessment report of the intergovernmental panel on climate change*. Available at: https://www.ipcc.ch/report/ar6/wg1/#TS.

Laskar, J., Robutel, P., Joutel, F., Gastineau, M., Correia, A. C. M., and Levrard, B. (2004). A long-term numerical solution for the insolation quantities of the Earth. *Astron. Astrophys.* 428 (1), 261–285. doi:10.1051/0004-6361:20041335

Li, Z., Gao, Y., and Han, L. (2017). Holocene vegetation signals in the alashan desert of northwest China revealed by lipid molecular proxies from calcareous root tubes. *Quat. Res.* 88 (1), 60–70. doi:10.1017/qua.2017.33

Li, Z., He, Y., and Chen, Q. (2018). Radiocarbon dating of aquatic gastropod shells and its significance in reconstructing quaternary environmental changes in the alashan plateau of northwestern China. *Geomorphology* 318, 18–25. doi:10.1016/j.geomorph.2018.06.002

Li, Z., Wang, N., Cheng, H., Ning, K., Zhao, L., and Li, R. (2015a). Formation and environmental significance of late quaternary calcareous root tubes in the deserts of the alashan plateau, northwest China. *Quat. Int.* 372, 167–174. doi:10.1016/j.quaint.2014.11.021

Li, Z., Wang, N., Li, R., Ning, K., Cheng, H., and Zhao, L. (2015b). Indication of millennialscale moisture changes by the temporal distribution of Holocene calcareous root tubes in the deserts of the alashan plateau, northwest China. *Palaeogeogr. Palaeoclimatol. Palaeoecol.* 440, 496–505. doi:10.1016/j.palaeo.2015.09.023

Liu, Z., Yang, X., and Zhu, B. (2010). Reinterpretation of the chronological data of palaeo-environmental records of the Badain Jaran Desert and reconstruction of the Holocene climatic. *Quat. Sci.* 30 (5), 925–933. doi:10.3969/j.issn.1001-7410.2010.05.10

Long, H., Shen, J., Tsukamoto, S., Chen, J.-H., Yang, L., and Frechen, M. (2014). Dry early Holocene revealed by sand dune accumulation chronology in bayanbulak basin (xinjiang, NW China). *Holocene* 24 (5), 614–626. doi:10.1177/0959683614523804

Lu, H., and Liu, K. (2003). Morphological variations of lobate phytoliths from grasses in China and the south-eastern United States. *Divers. Distrib.* 9 (1), 73–87. doi:10.1046/j.1472-4642.2003.00166.x

Lu, H., Wu, N., Liu, K., Jiang, H., and Liu, T. (2007). Phytoliths as quantitative indicators for the reconstruction of past environmental conditions in China II: Palaeoenvironmental reconstruction in the loess plateau. *Quat. Sci. Rev.* 26 (5–6), 759–772. doi:10.1016/j.quascirev.2006.10.006

Lu, H., Wu, N., Yang, X.-D., Jiang, H., Liu, K., and Liu, T. (2006). Phytoliths as quantitative indicators for the reconstruction of past environmental conditions in China I: Phytolith-based transfer functions. *Quat. Sci. Rev.* 25 (9–10), 945–959. doi:10.1016/j.quascirev.2005.07.014

Ma, C., Zhu, C., Zheng, C., Wu, C., Guan, Y., Zhao, Z., et al. (2008). High-resolution geochemistry records of climate changes since late-glacial from Dajiuhu peat in Shennongjia Mountains, Central China. *Sci. Bull. (Beijing).* 53 (26–37), 28–41. doi:10.1007/s11434-008-5007-6

Ma, N., Wang, N., Zhao, L., Zhang, Z., Dong, C., and Shen, S. (2014). Observation of megadune evaporation after various rain events in the hinterland of Badain Jaran desert, China. *Chin. Sci. Bull.* 59 (2), 162–170. doi:10.1007/s11434-013-0050-3

Ma, N., Wang, N., Zhu, J., Chen, X., Chen, H., and Dong, C. (2011). Climate change around the Badain Jaran desert in recent 50 years. *J. Desert Res.* 31 (6), 1541–1547. (in Chinese).

Mann, M. E., and Jones, P. D. (2003). Global surface temperatures over the past two millennia. *Geophys. Res. Lett.* 30 (15). doi:10.1029/2003GL017814

Moberg, A., Sonechkin, D. M., Holmgren, K., Datsenko, N. M., and Karlen, W. (2006). Highly variable northern Hemisphere temperatures reconstructed from low-and high-resolution proxy data. *Nature* 433 (7026), 613–617. doi:10.1038/nature03265

Mohtadi, M., Prange, M., and Steinke, S. (2016). Palaeoclimatic insights into forcing and response of monsoon rainfall. *Nature* 533 (7602), 191–199. doi:10.1038/nature17450

Ning, K., Li, Z., Wang, N., Sun, J., and Shao, W. (2013). Spatial characteristics of grain size and its environmental implication in the Badain Jaran desert. *J. Desert Res.* 33 (3), 642–648. doi:10.7522/j.issn.1000-694X.2013.00092

Ning, K., Wang, N., Lv, X., Li, Z., Sun, J., An, R., et al. (2019). A grain size and N-alkanes record of Holocene environmental evolution from A groundwater recharge lake in Badain Jaran desert, northwestern China. *Holocene* 29 (6), 1045–1058. doi:10.1177/0959683619831430

Ning, K., Wang, N., Yang, Z., Zhang, L., Wang, Y., Li, Z., et al. (2021). Holocene vegetation history and environmental changes inferred from pollen records of A groundwater recharge lake, Badain Jaran desert, northwestern China. *Palaeogeogr. Palaeoclimatol. Palaeoecol.* 577, 110538–110612. doi:10.1016/j.palaeo.2021.110538

Niu, Z., Wang, N., Meng, N., Liu, J., Liang, X., Cheng, H., et al. (2021). Contribution of lake-dune patterning to the dune height of mega-dunes in the Badain jaran sand sea, northern China. *Remote Sens. (Basel).* 13 (23), 4915. doi:10.3390/rs13234915

Peng, J., Dong, Z., Han, F., and Gao, L. (2016). Aeolian activity in the south margin of the Tengger Desert in northern China since the late glacial period revealed by luminescence chronology. *Palaeogeogr. Palaeoclimatol. Palaeoecol.* 457, 330–341. doi:10.1016/j.palaeo.2016.06.028

Qiao, Z., Jie, D., Liu, H., Ge, Y., and Zhang, H. (2010). Morphological characteristics and environmental implications of phytoliths in topsoils from different vegetation zones on northern slope of changbai mountains, China. *Chin. Geogr. Sci.* 20 (6), 506–512. doi:10.1007/s11769-010-0424-2

Stott, L., Cannariato, K., Thunell, R., Haug, G. H., Koutavas, A., and Lund, S. (2004). Decline of surface temperature and salinity in the western tropical pacific ocean in the Holocene epoch. *Nature* 431, 56–59. doi:10.1038/nature02903

Sun, J., Hu, W., Wang, N., Zhao, L., An, R., Ning, K., et al. (2018). Eddy covariance measurements of water vapor and energy flux over a lake in the Badain Jaran desert, China. *J. Arid. Land* 10 (4), 517–533. doi:10.1007/s40333-018-0057-3

Ter Break, C. J. F., and Juggins, S. (1993). Weighted averaging partial least squares regression (WA-PLS): An improved method for reconstructing environmental variables from species assemblages. *Hydrobiologia* 269, 485–502. doi:10.1007/BF00028046

Wang, H., Lu, H., Zhang, H., Yi, S., Gu, Y., and Liang, C. (2019). Grass habitat analysis and phytolith-based quantitative reconstruction of asian monsoon climate change in the sand-loess transitional zone, northern China. *Quat. Res.* 92 (2), 519–529. doi:10.1017/qua.2019.32

Wang, M., Dong, Z., Luo, W., Lu, J., Li, J., Cui, X., et al. (2015). Species diversity of vegetation and its relationship with soil characteristics in the southern marginal zone of the Badain Jaran desert. *Acta. Bot. Boreal.* 35 (2), 379–388. doi:10.7606/j.issn.1000-4025.2015.02.0379

Wang, N., Li, Z., Cheng, H., Li, Y., and Huang, Y. (2011). high lake levels on alxa plateau during the late quaternary. *Chin. Sci. Bull.* 56 (17), 1799–1808. doi:10.1007/s11434-011-4498-8

Wang, N., Ning, K., Li, Z., Wang, Y., Jia, P., and Ma, L. (2016). Holocene high lake-levels and pan-lake period on Badain Jaran Desert. *Sci. China Earth Sci.* 59 (8), 1633–1641. doi:10.1007/s11430-016-5307-7

Wang, T. (1990). Formation and evolution of badian jaran sandy desert, China. *J. Desert Res.* 10 (1), 29–40. (in Chinese).

Wang, Y., and Lu, H. (1993). *Phytolith study and its application*. Beijing: China Ocean Press.

Wanner, H., Beer, J., Butikofer, J., Crowley, T. J., Cubasch, U., Fluckiger, J., et al. (2008). Mid- to late Holocene climate change: An overview. *Quat. Sci. Rev.* 27 (19–20), 1791–1828. doi:10.1016/j.quascirev.2008.06.013

Wu, Y., Wen, X., and Zhang, Y. (2004). Analysis of the exchange of groundwater and river water by using radon-222 in the middle heihe basin of northwestern China. *Environ. Geol.* 45 (5), 647–653. doi:10.1007/s00254-003-0914-y

Xiao, J., Wu, J., Si, B., Liang, W., Nakamura, T., Liu, B., et al. (2006). Holocene climate changes in the monsoon/arid transition reflected by carbon concentration in Daihai lake of inner Mongolia. *Holocene* 16 (4), 551–560. doi:10.1191/0959683606hl950rp

Xiao, J., Xu, Q., Nakamura, T., Yang, X.-L., Liang, W., and Inouchi, Y. (2004). Holocene vegetation variation in the Daihai lake region of north-central China: A direct indication of the asian monsoon climatic history. *Quat. Sci. Rev.* 23, 1669–1679. doi:10.1016/j.quascirev.2004.01.005

Yang, B., Braeuning, A., Johnson, K. R., and Shi, Y. (2002). General characteristics of temperature variation in China during the last two millennia. *Geophys. Res. Lett.* 29 (9), 38-1–38-4. doi:10.1029/2001GL014485

Yang, X. (2000). Landscape evolution and precipitation changes in the Badain Jaran Desert during the last 30, 000 years. *Chin. Sci. Bull.* 45 (11), 1042–1047. doi:10.1007/BF02884988

Yang, X., Liu, T., and Xiao, H. (2003). Evolution of megadunes and lakes in the Badain Jaran desert, inner Mongolia, China during the last 31, 000 years. *Quat. Int.* 104 (1), 99–112. doi:10.1016/s1040-6182(02)00138-6

Yang, X., Ma, N.-N., Dong, J., Zhu, B., Xu, B., Ma, Z., et al. (2010). Recharge to the inter-dune lakes and Holocene climatic changes in the Badain Jaran Desert, western China. *Quat. Res.* 73 (1), 10–19. doi:10.1016/j.yqres.2009.10.009

Yang, X., Scuderi, L., Paillou, P., Liu, Z., Li, H., and Ren, X. (2011). Quaternary environmental changes in the drylands of China – a critical review. *Quat. Sci. Rev.* 30 (23–24), 3219–3233. doi:10.1016/j.quascirev.2011.08.009

Zhang, H., Wang, N., Li, Z., Dong, C., Lu, Y., and Li, G. (2011). Features of hydrogen and oxygen isotopes in lakes and groundwater in southeast Badain Jaran desert. *J. Desert Reasearch* 31 (6), 1623–1629.

Zhang, J., Jia, Y., Lai, Z., Long, H., and Yang, L. (2011). Holocene evolution of huangqihai lake in semi-arid northern China based on sedimentology and luminescence dating. *Holocene* 21 (8), 1261–1268. doi:10.1177/0959683611405232

Zhang, X., Hu, K., Fang, S., and Wang, D. (2008). Construction and application of phyolith-climate transfer functionin peat surface deposits of Northeast China. *Acta Sedimentol. Sinca* 26 (4), 138–144. (in Chinese).

Zhao, Y., Liu, H., Li, F., Huang, X., Sun, J., Zhao, W., et al. (2012). Application and limitations of the artemisia/chenopodiaceae pollen ratio in arid and semi-arid China. *Holocene* 22 (12), 1385–1392. doi:10.1177/0959683612449762

Zhao, Y., Yu, Z., Chen, F., and Li, J. (2008). Holocene vegetation and climate change from a lake sediment record in the tengger sandy desert, northwest China. *J. Arid. Environ.* 72 (11), 2054–2064. doi:10.1016/j.jaridenv.2008.06.016